

# Synthesis, Characterization, and Catalytic Activity of Heteroleptic Rhodium Complex for C–N Couplings<sup>1</sup>

M. N. Zafar<sup>a, \*</sup>, Fouzia Perveen<sup>b</sup>, A. Naz<sup>a</sup>, Ehsan Ullah Mughal<sup>c</sup>, Gul-e-Saba<sup>d</sup>, and K. Hina<sup>c</sup>

<sup>a</sup>Department of Chemistry, Quaid-i-Azam University, Islamabad, 45320 Pakistan

<sup>b</sup>RCMS, National University of Science and Technology, Islamabad, 44000 Pakistan

<sup>c</sup>Department of Chemistry, University of Gujrat, Gujrat, 50700 Pakistan

<sup>d</sup>Institute of Marine Biotechnology, University Malaysia, Terengganu, 21030 Malaysia

\*e-mail: analyticalc@yahoo.com

Received January 9, 2018; revised April 23, 2018; accepted June 15, 2018

**Abstract**—We have reported synthesis of complex [Rh(COD)(L{Me})Cl] (**III**), where L{Me} (**II**) is *N*-(1-methylpyridin-4(1*H*)-ylidene)benzamide and COD is 1,5-cyclooctadiene. Monodentate ligand L{Me} was synthesized by deprotonation of [HL{Me}][OTf] (**I**) with sodium hydride. [HL{Me}][OTf] was synthesised by methylation of *N*-(pyridin-4-yl)benzamide (HL) with methyl triflate. All the three synthesized compounds were characterized by FT-IR, NMR (<sup>1</sup>H and <sup>13</sup>C), elemental and MS analyses. The structure of complex **I** was further explored with single crystal XRD and computational studies. Complex **I** was found as a good catalyst for C–N coupling reactions. Molecular docking revealed strong binding of rhodium complex with myoglobin.

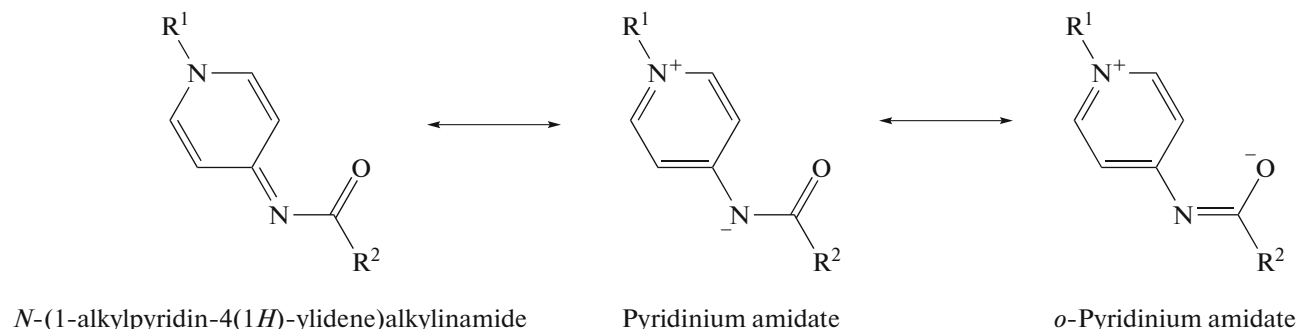
**Keywords:** *N*-(1-alkylpyridin-4(1*H*)-ylidene)amide, rhodium heteroleptic complex, density functional theory, molecular docking, myoglobin composites, C–N couplings

**DOI:** 10.1134/S1070328419010135

## INTRODUCTION

Owing to the high potential of N-heterocyclic carbenes (NHCs) as ligands in homogenous catalysis, the demand of ligands with similar structural and electronic features is obvious [1, 2]. A new

class of neutral ligand such as *N*-(1-alkylpyridin-4(1*H*)-ylidene) amide (PYA) with similar resonance structures is recently reported [3]. It can exist in three resonance forms are shown in Scheme 1:



**Scheme 1.**

<sup>1</sup> The article is published in the original.

Two with a negative charge associated with the donor atom (nitrogen or oxygen) and positive charge on pyridinium group. The third neutral resonance form shows negative charge in  $\pi$ -conjugation with a positively charged pyridinium group. It could have an influence on metal complex formation similar to NHCs as these ligands are less polar than anionic amidates themselves. Considering the fact that amidates are suitable for promoting oxidative addition reactions with the late transition metals [4–10] and the neutral nature of PYA can mimics metal–ligand equilibria of metal-NHC and metal-phosphine catalytic cycles, these ligands can be very powerful in homogenous catalysis. Rh(I)-NHC complexes have been successfully utilized for C–N and other cross coupling reactions [11–13]. Pd(II)-PYA complexes were utilized for C–C cross coupling reactions in our initial work [3]. Being non-innocent ligand in nature, its complexes with ruthenium such as Ru( $\eta^6$ -*p*-cymene)(PYA) and Ir( $\eta^5$ -cp\*)(PYA) showed (de)hydrogenation and water oxidation catalysis, respectively [14–16].

Composites of proteins and metal complexes are attractive biomolecules as they act as sensors for biomarkers [17, 18] and are artificial catalysts [19–21]. Various key biomarkers play an important role to predict disease susceptibility and assist in its management. Myoglobin is an important cardiac biomarker that is released into the bloodstream after induction of muscle injury within 1 h and reaches its peak levels after 2 h and thus an early indicator of acute myocardial infarction [22, 23]. It can be monitored by quick spectroscopic test of blood sample after addition of organometallic precursor that can strongly interact with this protein [24–26]. The other aspect of incorporation of catalytically active metal complexes in well-characterized stable proteins is with respect to the preparation of artificial metalloenzymes having non-natural functions [27–31]. The resulting hybrid catalysts combine attractive features of both homogeneous and enzymatic systems. There are many examples of encapsulation of biotinylated metal complexes into protein cavity through specific interactions [32–34]. Biotinylated rhodium complex, [Cp\* $\text{RhCl}_2$ ]<sub>2</sub>, in streptavidin was utilized for accelerated asymmetric C–H activation. Rhodium complexes with chiral (*S,S*)-Phebox complexes with different alkyl substituents on the oxazoline rings such as Me, Et, *i*-Pr, Ph, and Bn were successfully incorporated in apo-myoglobin and the composites formed were found to be good catalysts for hydrosilylation of monosubstituted and disubstituted alkenes [35]. Literature clearly revealed that compounds having aromatic ring, hydrophobic moiety, donor and acceptor sites are essential for their binding with myoglobin protein [32–35].

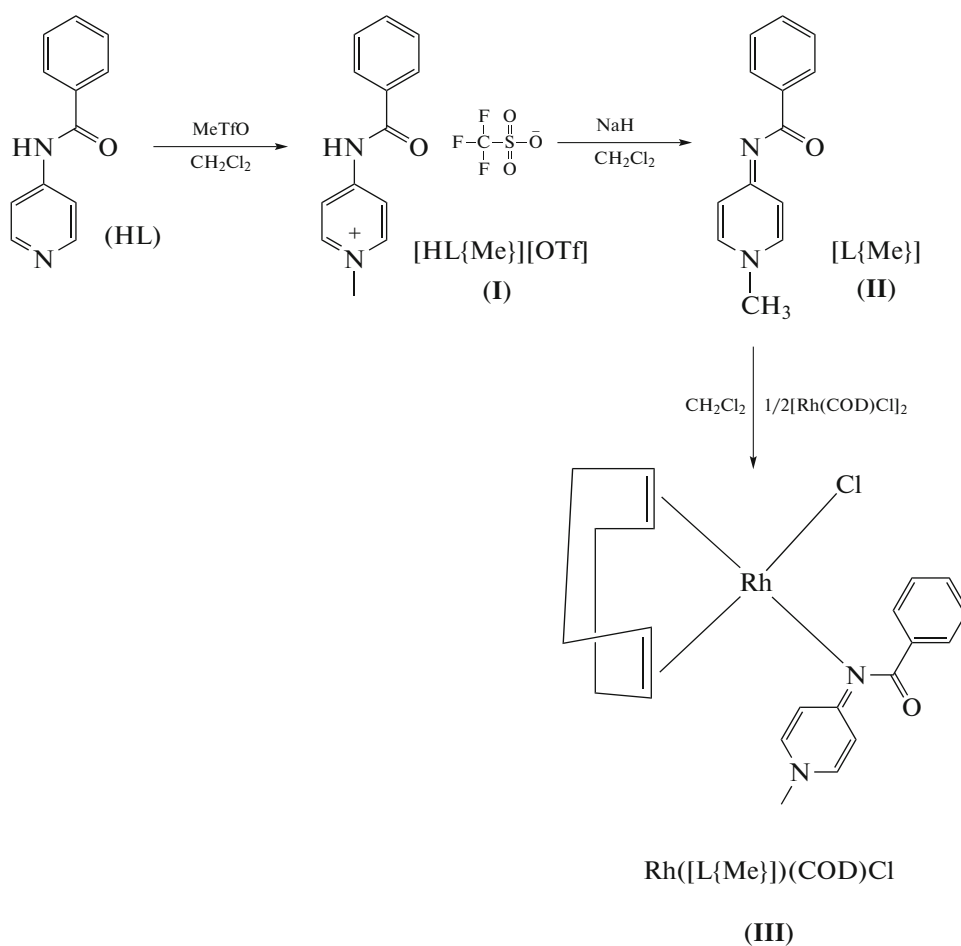
In this current work, monodentate pyridinium amidate, [L{Me}] (II), protonated pyridinium amidate, [HL{Me}][OTf] (I), as well as its rhodium complex [Rh(COD)(L{Me})Cl] (III), were synthesized and characterized. The structure of I was further explored by single crystal XRD and density functional theory (DFT) methods. It includes electronic properties, excitations, molecular electrostatic potential (MEP), energies of chemical states and docking studies with myoglobin. It has been developed in several studies that electronic and geometric properties calculated by DFT methods are far more reliable than semi-empirical methods [36, 37]. Complex III was also utilized as a catalyst for C–N coupling reactions owing to low oxidation state of Rhodium bonded with electron donor ligands.

## EXPERIMENTAL

**Materials and instrumentation.** All reactions were performed using standard Schlenk techniques and utilized moisture free nitrogen environment unless otherwise noted. Solvents and liquid reagents were distilled under nitrogen. Dichloromethane was dried using a MBRAUN MB SPS-800 solvent purifier and stored under nitrogen. Water was used deionized and reagents were used as received. 4-Chloro-1-methylpyridin-1-ium triflate was prepared by our previous reported method [38].

Infrared spectra were recorded over the range 4000–400  $\text{cm}^{-1}$  on a Perkin Elmer Spectrum 400 FT-IR spectrometer. NMR spectra were obtained using a Bruker Avance spectrometer at 300 MHz ( $^1\text{H}$ ) and 75 MHz ( $^{13}\text{C}$ ) at 300 K at 298K.  $^1\text{H}$  spectra were referenced to TMS (0.00 ppm), or protio impurity of DMSO- $d_6$  (2.50 ppm) or  $\text{CDCl}_3$  (5.70 ppm).  $^{13}\text{C}$  NMR spectra were referenced to  $\text{CDCl}_3$  (77.0 ppm) or DMSO (39.43 ppm). The numbering scheme used for interpreting NMR spectras is same as that used for XRD of [Rh(COD)(L{Me})Cl]. Mass spectra were recorded on a Bruker micrOTOF QII quadrupole-time-of-flight mass spectrometer. Elemental analyses for C, N, and H were performed at the Campbell Microanalytical Laboratory, University of Otago. X-ray crystal structures were solved by the Siemens SMART APEX II diffractometer. Intensity data were collected at 293 K using  $\text{MoK}_\alpha$  radiation.

Synthesis of ligands and Rh complex is shown in Scheme 2:



Scheme 2.

**Synthesis of *N*-(pyridin-4-yl)benzamide (HL).** 4-Aminopyridine (1.52 g, 16.3 mmol) and triethylamine (3.40 mL, 24.5 mmol, 1.5 eqv.) were combined in dichloromethane (300 mL) under nitrogen, giving a colourless suspension. Benzoyl chloride (2.30 g, 16.3 mmol) in dichloromethane (75 mL) was added drop wise with stirring via a pressure equalizing dropping funnel over a period of 30 min and the solution stirred for a total of 4 h. After this time, the solvent was evaporated and solid was collected and washed with cold water (5 mL). Finally the solid product was dried under high vacuum to give HL (2.66 gm, 83%) which was used in subsequent reactions without further purification. All characterisation data of this compound was obtained as previously reported [39].

**Synthesis of [HL{Me}][OTf] (I).** HL (250 mg, 1.26 mmol) was placed in a 25 mL three-necked round-bottomed flask fitted with a condenser and the flask evacuated. An atmosphere of dry nitrogen was re-established and the flask was charged with anhydrous dichloromethane (15 mL), forming white suspension. Methyl triflate (428  $\mu\text{L}$ , 3.78 mmol, 3 eqv.)

was added dropwise over a period of ~2 min causing the suspension to become gelatinous. The reaction mixture was heated under reflux for 30 min, then cooled to ambient temperature and filtered. The solid was washed successively with dichloromethane (25 mL) and then with hexane (10 mL) and finally dried in vacuo to give pure I (434 mg, 95%).

For  $\text{C}_{14}\text{H}_{13}\text{N}_2\text{O}_4\text{F}_3\text{S} \cdot 1/2\text{H}_2\text{O}$

Anal. calcd., %	C, 45.28	H, 3.80	N, 7.54
Found, %	C, 45.56	H, 3.67	N, 7.65

IR ( $\nu$ ,  $\text{cm}^{-1}$ ): 3310 w, 3068 w, 1690 m, 1648 m, 1519 m, 1463 m, 1321 m, 1293 m, 1240 s, 1171 m, 1028 s, 855 m, 702 m, 515 s.  $^1\text{H}$  NMR (DMSO- $d_6$ , 300 MHz;  $\delta$ , ppm ( $J$ , Hz)): 11.51 (s., 1H, NH), 8.76 (d., 2H,  $^3J_{\text{HH}} = 6.9$ , H18, 19), 8.29 (d., 2H,  $^3J_{\text{HH}} = 7.2$ , H20, 17), 8.03 (d., 2H,  $^3J_{\text{HH}} = 8.4$ , H15, 11), 7.74–7.64 (m., 3H, H14, 12), 4.19 (s., 3H, H21).  $^{13}\text{C}$  NMR (DMSO- $d_6$ , 75 MHz;  $\delta$ , ppm): 167.15 (C9), 151.88 (C16), 145.80 (C19, 18), 133.09 (C13), 132.86 (C10), 128.66 (C14, 12), 128.21 (C15, 11), 115 (C20, 17),

46.31 (C21). Mass spectrometry (ESI): molecular ion  $[C_{13}H_{13}N_2O]^+$   $[M - CF_3SO_3^-]^+$  mass calcd. 213.1028, mass found 213.1022.

**Synthesis of  $[L\{Me\}]$  (II).** To a stirred suspension of **I** (200 mg, 552  $\mu$ mol) in 10 mL of dichloromethane at room temperature was added NaH (66 mg, 2.76 mmol, 5 eqv.). The solution was stirred for 5 h and after filtration through celite, the solvent was removed under vacuum to afford a colourless glass. The solid was recrystallised from dichloromethane and hexane to obtain analytically pure product. The resulting colorless microcrystalline solid was collected by filtration, washed with *n*-hexane (~20 mL) and dried *in vacuo* to give pure **II** (111 mg, 95%).

For  $C_{13}H_{12}N_2O \cdot 5/3H_2O$

Anal. calcd., %	C, 70.00	H, 5.96	N, 12.56
Found, %	C, 69.87	H, 5.69	N, 12.11

IR ( $\nu$ ,  $cm^{-1}$ ): 2956 w, 1646 m, 1586 m, 1551 m, 1488 s, 1425 m, 1347 s, 1306 m, 1260 m, 1260 m, 1190 m, 1166 s, 1018 m, 873 m, 733 m, 674 m, 518 m, 400 m.  $^1H$  NMR ( $CDCl_3$ , 300 MHz;  $\delta$ , ppm (*J*, Hz)): 8.24–8.21 (m., 2H, Ph), 7.54–7.52 (m., 2H, H19, 18), 7.43–7.36 (m., 2H, H20, 17 and Ph), 3.74 (s., 3H, H21).  $^{13}C$  NMR ( $CDCl_3$ , 75 MHz;  $\delta$ , ppm): 176.70 (C9), 164.71 (C16), 139.91 (C20, 17), 139.15 (C10), 130.66 (C13), 129.13 (C19, 18), 127.78 (C14, 12), 118.73 (C15, 11), 44.19 (C21). Mass spectrometry (ESI): molecular ion  $[C_{13}H_{13}N_2O]^+$   $[M + H]^+$  mass calcd. 213.1027; mass found 213.1022.

**Synthesis of  $[Rh(COD)(L\{Me\})Cl]$  (III).**  $[Rh(COD)Cl]_2$  (40 mg, 0.10 mmol) was added to a Schlenk tube containing a solution of **II** (59.26 mg, 0.20 mmol) in toluene (5 mL) and the solution was stirred for 10 min at room temperature. The product was filtered as a yellow-white powder (94 mg, 95%). Crystals of the product were grown in deuteriochloroform in a NMR-tube.

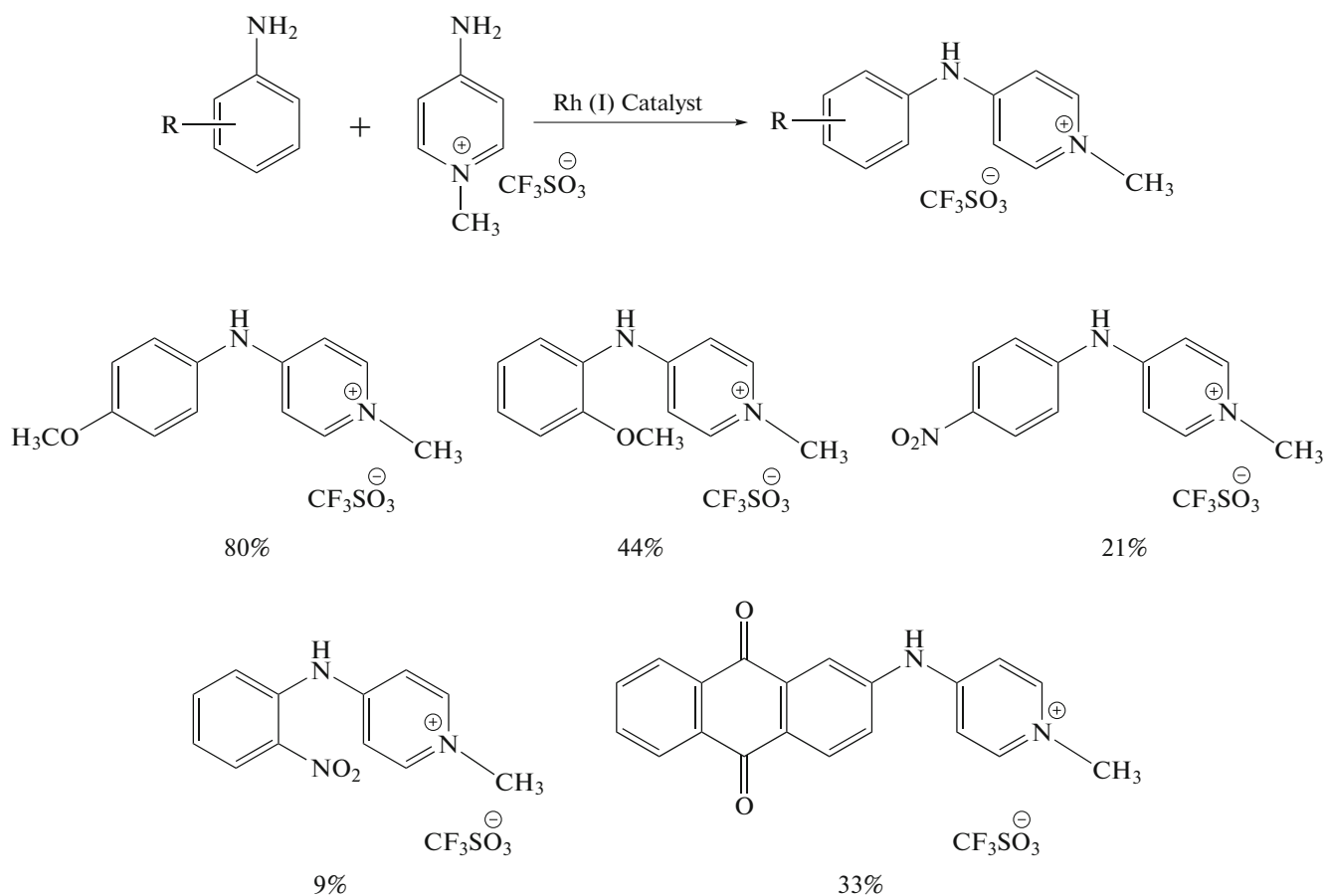
$^1H$  NMR ( $CDCl_3$ , 300 MHz;  $\delta$ , ppm (*J*, Hz)): 8.2–8.1 (d.d., 1H, arom.), 7.4–7.3 (m., 2H, arom.), 7.2–7.1 (m., 4H, arom.), 6.7–6.6 (d.d., 1H, arom.), 5.8–5.9 (d.d., 1H, arom.), 4.5 (m., 2H, cod CH), 3.51–3.49 (m., 5H,  $CH_3$  & cod CH), 2.35 (m., 4H, cod  $CH_2$ ), 1.63 (m., 4H, cod  $CH_2$ ).  $^{13}C$  NMR ( $CDCl_3$ , 75 MHz;  $\delta$ , ppm): 159.1, 148.9, 137.3, 137.2, 129.2, 124.8, 124.3, 122.2, 116.6, 109.3, 82.8 (cod), 77.4 (cod), 42.7, 31.1 (cod), 30.4 (cod).

**Computational study.** *Geometry optimizations pure QM computations.* All computations were carried out

using the Amsterdam Density Functional (ADF) 2007 suite of program [40]. Molecular geometry and energies of **I** were computed using the generalized gradient approximation (GGA) with the B3LYP functional [41, 42]. The molecular orbitals (MOs) were expanded in uncontracted sets of Slater type orbitals (STOs) containing diffuse functions with two sets of polarization functions (TZ2P) [43]. The 1s core shells of carbon, nitrogen and oxygen and 4p core shell Rh were treated by the frozen-core approximation. Rh complex geometries were optimized in the gas phase assuming  $C_{2v}$  symmetry. Mulliken population analysis was an importance property determined to calculate the degree of charge transfer (CT).

**Molecular docking methodology.** The RCSB Protein Data Bank (PDB) [44] was used to download the crystal structure of apo-A71G Myoglobin (PDB, ID: 2EF2). Myoglobin PDB coordinates with lowest energy and constant conformation were optimized by molecular dynamic AMBER force field for docking studies. No water molecules were involved in PDB molecule. MOPAC 7.0 was used to optimize energy of the additional hydrogen atoms to obtain a standard geometry of the structure. The subsequent structure was exposed to systematic conformational search at default parameters with RMS gradient of 0.01 kcal mol $^{-1}$  using Site Finder to find out active sites of protein. Scoring function was used as basis for final docking. Different docking runs were used to get precise binding docking poses. At each step of the simulation, the energy of interaction of compound with myoglobin was calculated. The remaining parameters were set as default.

**C–N Coupling methodology.** A mixture of the corresponding 4-chloro-1-methylpyridin-1-ium triflate (1.1 eqv.), substituted aromatic amine (1 eqv.), anhydrous potassium carbonate (3 eqv.) and  $[Rh(COD)(L\{Me\})Cl]$  (1.0 mol %) was refluxed in isopropyl alcohol (5 mL) for 6 h under nitrogen atmosphere. After this time, reaction mixture was cooled and then filtered to remove potassium carbonate. Solvent was removed from filtrate under low pressure. The solid obtained was washed thoroughly with dichloromethane and diethyl ether (5 mL each) to remove unreacted amine. Products were purified by flash chromatography on silica gel using methanol–dichloromethane (1 : 2) mixture as a mobile phase. and reactions are summarized along with the yield of the products in Scheme 3:



Scheme 3.

## RESULTS AND DISCUSSION

The protonated pyridinium amidate triflate salt,  $[HL\{Me\}][OTf]$  (**I**), was synthesized by treatment of HL with methyl triflate in anhydrous dichloromethane solution under reflux. The maximum product precipitated out from the reaction medium in half an hour. Examination of the IR spectrum of **I** showed a band at  $3310\text{ cm}^{-1}$ , which is assigned to  $\nu(N-H)$ . The amide band of this compound was observed at  $1690\text{ cm}^{-1}$ . Absorptions assigned to the triflate anion were observed at  $1293$ ,  $1240$  and  $1171\text{ cm}^{-1}$   $\nu(S=O)$  and  $1028\text{ cm}^{-1}$   $\nu(C-F)$ . The  $^1H$  NMR (DMSO- $d_6$ ) spectrum of **I** has a singlet at 11.51 ppm assigned to the amide proton. The N-methyl resonance in this compound was observed at 4.19 ppm.

To determine whether the cationic N-methyl pyridinium compound **I** could be converted into the corresponding neutral compound,  $[HL\{Me\}][OTf]$  was stirred with sodium hydride in dichloromethane solvent at room temperature. After 5 h, the solution was filtered and the solvent was removed under vacuum

affording the white deprotonated pyridinium amidate,  $[L\{Me\}]$  (**II**), product. To find out the reactivity of **II**, it was tested under different conditions as summarized in Table 1. It was found out that it was protonated, upon their treatment with triflic acid in DMSO solvent. It did not react with refluxed methanol and water at room temperature. However, it hydrolyzed fully upon treatment with refluxed water for 6 h. Signals assignable to  $\nu(S=O)$  and  $\nu(C-F)$  were absent from the IR spectrum of **II**, confirming that triflate ion was not present. The band that was observed at  $1690\text{ cm}^{-1}$  in **I** was replaced by a new band at  $1646\text{ cm}^{-1}$ . The high resolution mass spectrum (ESI $^+$ ,  $[M + H]^+$ ) of the product showed base peak at  $m/z$  213.1022. The NMR spectrum of **II** was markedly different to that of **I**. Critically, signals attributable to amide NH group were absent from the  $^1H$  NMR and IR spectra. The N-methyl resonance was observed at 3.83 ppm, which is shifted upfield from the corresponding signal for **I** where it is observed at 4.19 ppm. It was also found that the  $^1H$  NMR spectrum for **II** displays two multiplets rather than doublets for four proton (H9-12) in

**Table 1.** Reactivity of [L{Me}]

Reaction conditions	Observations and results
Solid was treated to Triflic acid (1 : 2) in DMSO	Protonated
20 mg of solid was dissolved in methanol and the solution was refluxed for 30 mins. After that the solvent was removed under reduced pressure using a rotary evaporator at 40°C	No reaction
20 mg of solid was dissolved in 0.75 mL of DMSO containing few drops of water and was left for 48 h	No hydrolysis
20 mg of solid was dissolved in a 1 mL solution containing 10% H <sub>2</sub> O/THF and was refluxed. After that the solvent was removed under vacuum on a rotary evaporator at 40°C (5 min)	No hydrolysis of ligand occur even after two hours
20 mg of solid was suspended 1 mL H <sub>2</sub> O and was refluxed for about 6 h. After that the solvent was removed under vacuum on a rotary evaporator at 40°C	Fully hydrolyzed and resulted in benzoate anion and corresponding cation

the pyridinium ring, owing to the considerable double-bond character and restricted rotation of the C(16)–N(1) bond. Johnson also found this restricted rotation of the exocyclic C–N bond for pyridinium amide ligand that resulted in four proton environments (H17–20) for the nitrogen containing ring [45].

[Rh(COD)(L{Me})Cl][OTf] was synthesized via the similar path used by Hermann for carbenes [46]. [Rh(COD)Cl]<sub>2</sub> was used as rhodium source owing to its solubility in toluene that was allowed to react with [L{Me}] in a Schlenk tube. The yellow product, formed in excellent yield within 10 min, filtered as a yellow-white powder. The <sup>1</sup>H NMR of the complex showed aromatic signals in the extended range of 8.2–6.0 ppm as compared to [L{Me}], 8.2–7.4 ppm. Similarly trend of aromatic signals is shown in the <sup>13</sup>C NMR of the complex (159.1–109.3 ppm) as compared to [L{Me}] (176.7–118.7 ppm). In addition, Rhodium coordinated cyclooctadiene showed four signals, more shielded methylene appeared upfield and less shielded methine appeared downfield like in case of [Rh(COD)(NHC)Cl] [47]. Signals due to methyl are also shifted as compare to protonated and deprotonated ligands. Crystals of the product were grown in deuteriochloroform in an nmr tube. An ORTEP depiction is shown in Fig. 1.

DFT studies were performed on the Rh(L{Me})(COD)Cl (**III**) to gain a greater insight into the structural and electronic changes that occur upon deprotonation and complexation of **I** with rhodium precursor. Calculated and experimental bond lengths as well as angles of **III** are compared in Tables 2 and 3. The results showed best agreement with experimental determined values given that some differences are expected between the solid-state and gas-phase structures. Analogous to the DFT calculations, X-ray structures confirmed significant structural changes occur upon deprotonation and complexation of [HL{Me}][Cl] to form **III**. There is a shortening of C(16)–N(1) (1.37 Å) compared to normal

C–N (1.39 Å) [3] in amide ligand. Similarly C(17)–C(18), C(19)–C(20), shortened compared to C(16)–C(20) and C(16)–C(17) (by 0.04 and 0.05 Å respectively), suggesting that *N*-(1-methylpyridin-4(*1H*)-ylidene)benzamide resonance structure is more predominant.

Energies of frontier molecular orbitals, i.e., HOMO and LUMO energies, are significantly important characteristic parameters for electronic structure methods. LUMO represents electron accepting characteristics of a molecule, whereas HOMO denotes the capability of a molecule to donate an electron [48]. A critical parameter in determining molecular stability and electrical transport properties is energy gap ( $\Delta E$ ) between HOMO and LUMO.  $\Delta E$  is also a measure of electron conductivity of a compound as well [49]. Figure 2 reveals the patterns of the HOMO and LUMO of **III** calculated with the B3LYP functional. The positive phase is symbolized with blue and the negative phase orange. HOMO and LUMO energies of the **III** are also listed along with their molecular orbitals. It can be seen that the HOMO and LUMO of Rh(L{Me})(COD)Cl are –5.7255 and –5.0363 eV, respectively, which shows ( $\Delta E$ ) was found to be –0.6892 eV. Figure 3 depicts that it is easier for the vertical transitions from the 1s of Rh and 2p of N to jump from HOMO to LUMO due to smaller band gap.

To further apprehend the electronic transitions of Rh(L{Me})(COD)Cl, TDDFT/B3LYP DZ was applied to investigate the nature and the energy of absorption spectra on the basis of the optimized geometry. The electronic absorption spectrum was simulated by the Double zeta basis functions with the singlet energies from calculations. Figure 4 depicts the electronic transition for the singlet excited state compound exhibiting  $\lambda_{\max}$  at 630 nm other important transitions to be at 520 and 280 nm.

In the field of quantum chemistry, calculation of effective atomic charges play a significant role in the application of molecular systems. The MPA shows

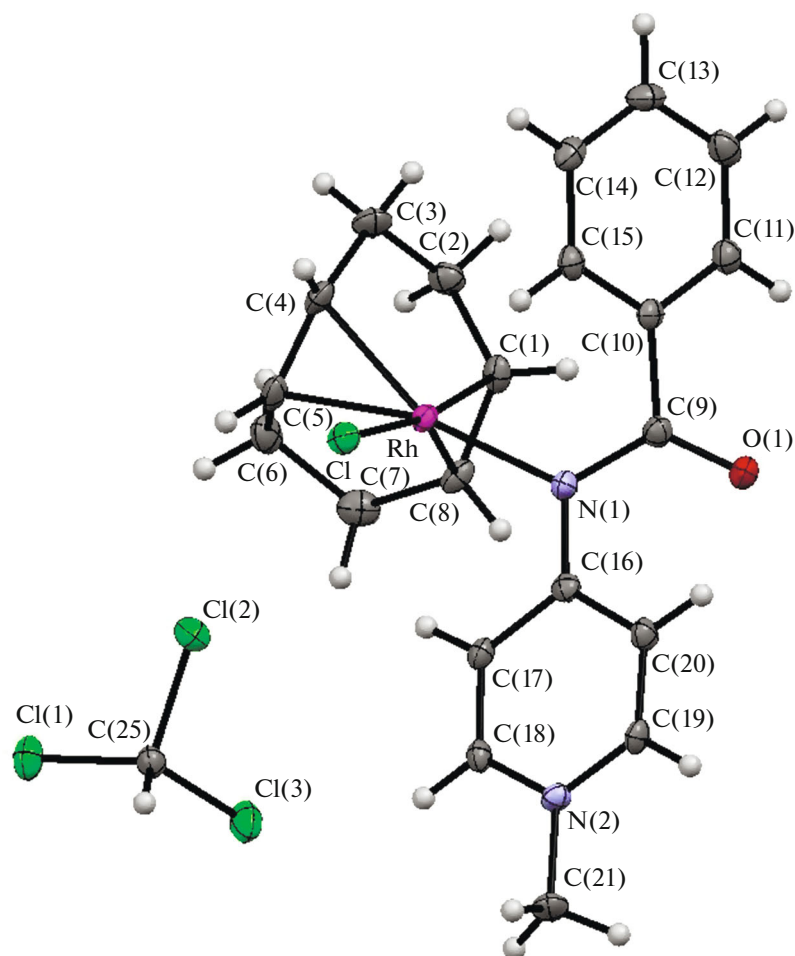


Fig. 1. ORTEP diagram of Rh(L{Me})(COD)Cl (III).

(Fig. 5, Table 4), that presence of two N-atoms, i.e.,  $N(1) = -0.572$ ,  $N(2) = -0.486$  and one O-atom,  $O(1) = 0.570$ , imposes distribution large positive charges on  $C(9) = 0.544$ . Alternatively all C-atoms of aromatic ring possess negative charges due to delocalization of  $\pi$ -electrons. Importantly highly electropositive atom with Mulliken charge distribution is  $Rh = 0.517$  due to  $N(1)$ . All hydrogen atoms have positive charge distribution.

The MEP map is a convenient way to investigate the electrophilic and nucleophilic regions [50]. MEP demonstrates molecular size, shape, positive, negative and neutral regions based on color grading. In Fig. 6, MEP displays the most negative region associated with the lone pair of  $N(1)$  followed by  $O(1)$  atom. MEP increases in the order of red, orange, yellow, green, blue. The areas having excess of electrons are represented by negative potential with red and yellow

Table 2. Selected bond lengths ( $\text{\AA}$ ) for  $[\text{Rh}(\text{L}\{\text{Me}\})(\text{COD})\text{Cl}]$  determined by X-ray diffraction method and DFT calculations

Bond lengths	XRD	DFT	Bond lengths	XRD	DFT	Bond lengths	XRD	DFT
Rh–Cl	2.39	2.38	C(9)–N(1)	1.38	1.40	C(17)–C(18)	1.36	1.37
Rh–N(1)	2.14	2.14	C(9)–O(1)	1.23	1.22	C(18)–N(2)	1.34	1.34
Rh–C(1)	2.12	2.14	C(10)–C(11)	1.39	1.40	C(19)–N(2)	1.35	1.34
Rh–C(4)	2.12	2.14	C(16)–N(1)	1.37	1.39	C(19)–C(20)	1.36	1.39
Rh–C(5)	2.14	2.13	C(16)–C(17)	1.41	1.41	C(21)–N(2)	1.48	1.41
Rh–C(8)	2.10	2.14	C(16)–C(20)	1.41	1.41	C(1)–C(8)	1.41	1.40

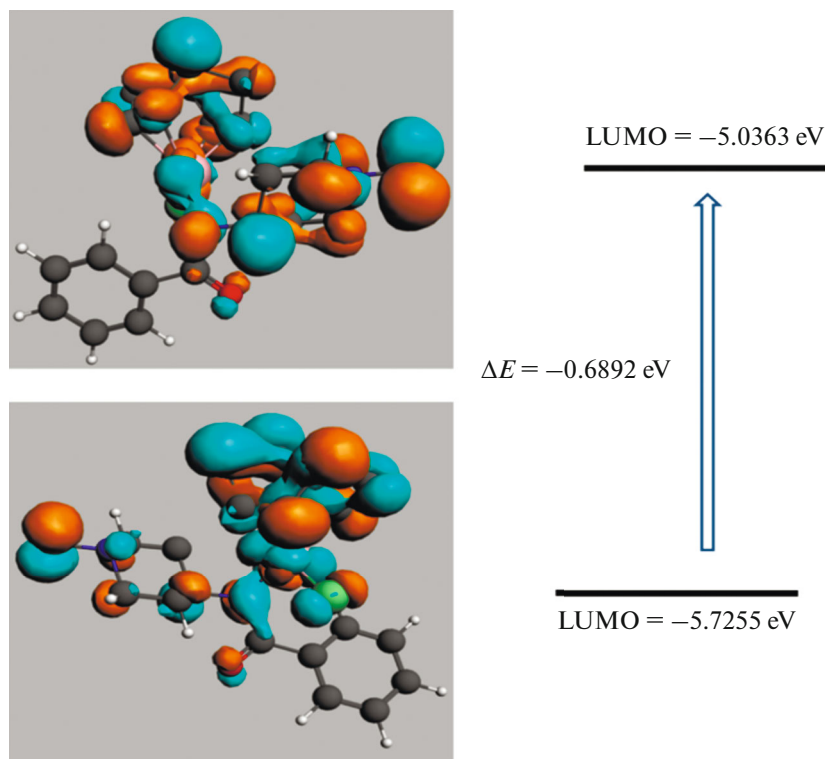
**Table 3.** Selected bond angles (deg) for title compound [Rh(L{Me})(COD)Cl] determined by X-ray diffraction and DFT calculations

Bond angles	XRD	DFT	Bond Angles	XRD	DFT
ClRhN(1)	89.24	89.20	C(12)C(13)C(14)	120.1	118.0
C(4)RhC(8)	98.7	97.7	N(1)C(9)O(1)	124.8	124.0
C(4)RhCl	91.9	96.5	C(11)C(10)C(15)	119.5	120.0
C(9)N(1)C(16)	118.5	118.0	C(20)C(19)N(2)	121.8	120.5
C(21)N(2)C(19)	120.2	120.0	C(16)C(17)C(18)	120.7	119.9
C(9)C(10)C(15)	122.3	122.1	C(18)N(2)C(19)	119.5	120.5
N(1)RhC(1)	93.2	92.0	C(18)N(2)C(21)	120.2	119.9
C(9)C(10)C(11)	119.1	120.7	C(19)C(20)H(20)	119.6	120.9
C(11)C(12)C(13)	119.7	120.4	C(17)C(16)C(20)	115.6	115.0
O(1)C(9)C(10)	119.1	119.0	C(17)C(18)N(2)	121.6	120.5

color (C=C group, oxygen and nitrogen atoms), whereas electron deficient regions are expressed by the regions having the positive potential with hydrogen atoms.

From molecular docking analysis of myoglobin protein targets with **III** using docking procedure, it can be deduced that intermolecular hydrophobic and stacking interactions are involved in stabilizing the computationally predicted lowest energy adduct. Minimum binding free energy and lowest root mean

square deviations were selected for docking pose of the compound. Rh complex interacts with amino acid residues like His 93, Phe 138, Leu 104, Ile 107, Ile 99, Leu 72, Leu 29, Phe 43, His 64, Val 68, Thr 67 and Leu 89 of 2EF2 pocket via van der Waals interactions as illustrated in Fig. 7. Binding strength ( $K_b$ ) of Rh complex with 2EF2 was calculated from Gibbs free energy ( $\Delta G$ ) of complexation, which showed significant binding affinity between two. Moreover, negative value of  $\Delta G$  indicates that interaction process of Rh

**Fig. 2.** Surfaces of the frontier molecular orbitals Rh(L{Me})(COD)Cl using the generalized gradient approximation (GGA) with the B3LYP functional.

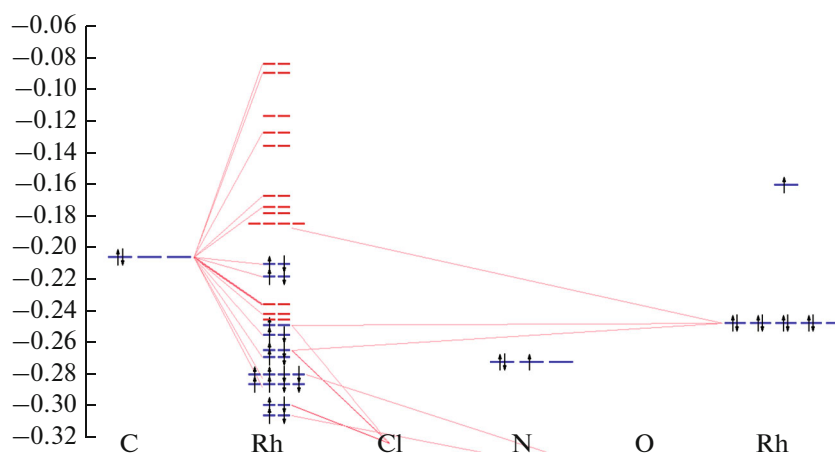


Fig. 3. Energy level diagram of III using the generalized gradient approximation (GGA) with the B3LYP.

complex with 2EF2 is spontaneous [51]. Binding constant, free energy and other calculated parameters (octanol/water partition coefficient (P), molar refractivity (MR) and van der Waals (VDW) surface area are given below:

Free energy $\Delta G$ , $\text{kJ mol}^{-1}$	Binding constant $K_b$ , $\text{M}^{-1}$	Slog P	MR	VDW
-17.48	$1.158 \times 10^3$	5.096	9.94	383.54

To gauge the potential utility of the PYA ligand as supporting ligands, preliminary C–N cross-coupling experiments with  $[\text{Rh}(\text{COD})(\text{L}\{\text{Me}\})\text{Cl}][\text{OTf}]$  were carried out. The results obtained for coupling of various substituted amines with 4-chloro-1-methylpyridin-1-ium triflate are mentioned in Scheme 3. Maximum yield was obtained for 4-methoxyaniline and least for 2-nitroaniline. The lone pair on 4-methoxy-substituted on aniline enhances the nucleophilic character of amine by resonance effect. The electron withdrawing substituted nitro deactivates the aniline. It is

also observed that *ortho* analogues of amines are less active than *para*, owing to more steric bulk close to aniline nitrogen that can hinder its reactivity with 4-chloro-1-methylpyridin-1-ium triflate. 2-Aminoanthracene-9,10-dione yield 33% of product due to electron withdrawing carbonyl groups on anthracene ring.

In summary, neutral monodentate nitrogen donor *N*-(1-methylpyridin-4(1*H*)-ylidene)benzamide (PYA) ligand was synthesized by abstraction of proton from its protonated triflate salt,  $[\text{HL}\{\text{Me}\}][\text{OTf}]$ , with sodium hydride.  $[\text{Rh}(\text{COD})(\text{L}\{\text{Me}\})\text{Cl}]$  was synthesized by addition of PYA ligand to  $[\text{Rh}(\text{COD})\text{Cl}]_2$  in dichloromethane solvent. Single crystal of  $[\text{Rh}(\text{COD})(\text{L}\{\text{Me}\})\text{Cl}]$  was successfully grown and its structure was determined. Geometric parameters obtained by this method were found comparable with DFT results. HOMO and LUMO energy analysis, MEP, Mulliken atomic charges and electronic properties of the Rh complex have been calculated by using generalized gradient approximation (GGA) with B3LYP functional method. HOMO and LUMO

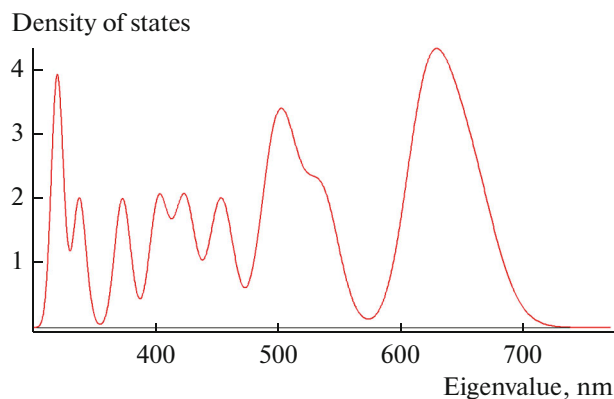
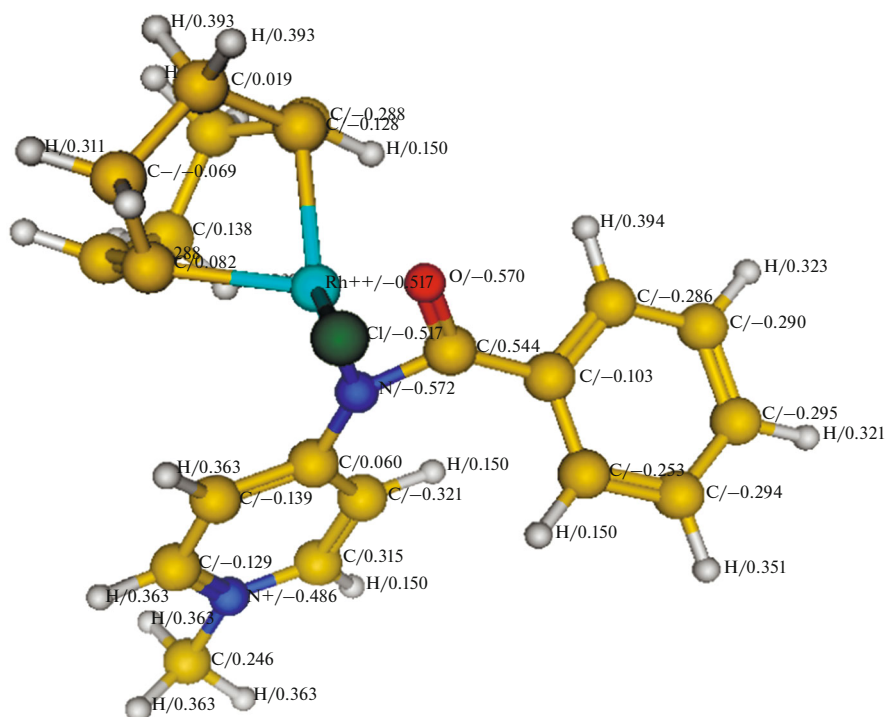
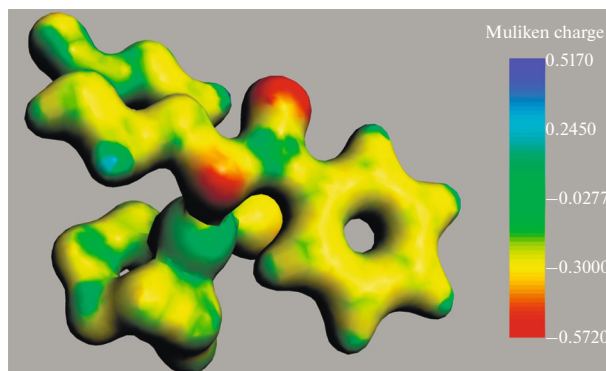


Fig. 4. Energy level plot of III using the generalized gradient approximation (GGA) with the TDDFT/B3LYP DZ.



**Fig. 5.** Optimized molecular geometry and Mulliken population charges of **III** using the generalized gradient approximation (GGA) with the B3LYP functional.



**Fig. 6.** Molecular electrostatic potential (PES) of Rh(L{Me})(COD).

energy gap indicated the eventual charge transfer interactions taking place within the molecule. Strong interaction of [Rh(COD)(L{Me})Cl] with myoglobin

protein, a potential biomarker of acute myocardial infection, suggests its potential as myoglobin sensor and as an artificial enzyme. [Rh(COD)(L{Me})Cl]

**Table 4.** Mulliken population analysis of [Rh(L{Me})(COD)Cl] using the generalized gradient approximation (GGA) with the B3LYP functional

Atoms	Charge analysis	Atoms	Charge analysis	Atoms	Charge analysis
Rh	0.517	Cl	-0.015	C(12)	-0.294
N(1)	-0.572	C(9)	0.544	C(16)	0.060
N(2)	-0.486	C(14)	-0.290	H(19)	0.150
O(1)	-0.570	C(13)	-0.295	H(20)	0.150

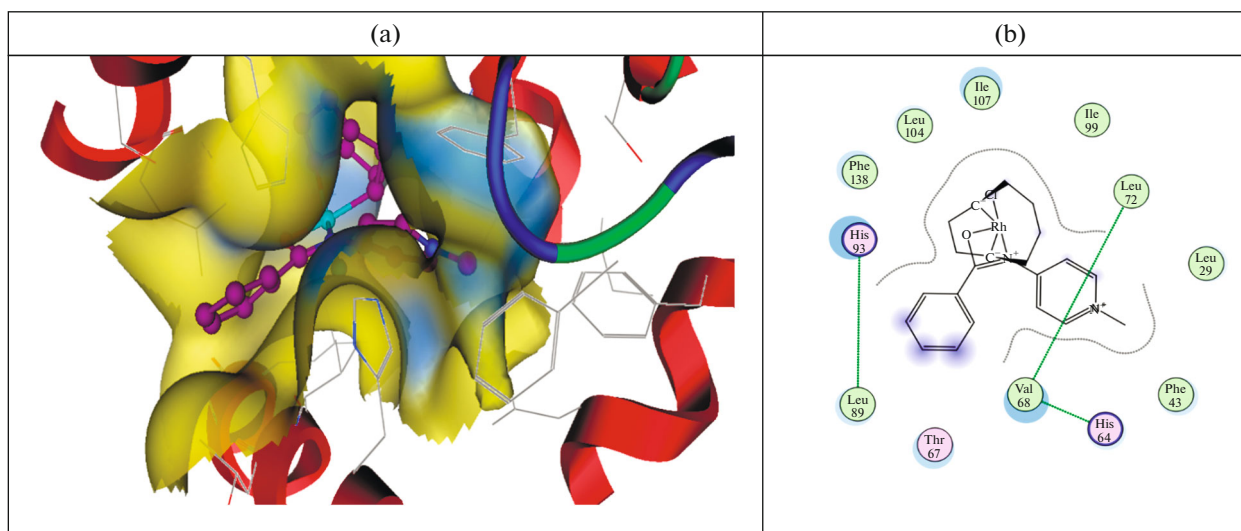


**Fig. 7.** Visuals of docking interactions of Rh complex with 2EF2 enzyme (a), 2D ligplots showing interactions of amino acid residues of 2EF2 with Rh complex (b).

also proved to be a good catalyst for C–N coupling reactions. Electron donor *para*-substituted amines were found to be most active to couple with 4-chloro-1-methylpyridin-1-ium triflate.

#### REFERENCES

- Hopkinson, M.N., Richter, C., Schedler, M., and Glorius, F., *Nature*, 2014, vol. 510, p. 485.
- Peris, E., *Chem. Rev.*, 2017. doi 10.1021/acs.chemrev.6b00695
- Boyd, P.D.W., Wright, L.J., and Zafar, M.N., *Inorg. Chem.*, 2011, vol. 5, p. 10522.
- Redmore, S.M., Rickard, C.E.F., Webb, S.J., and Wright, L.J., *Inorg. Chem.*, 1997, vol. 36, p. 4743.
- Zhang, J., Liu, Q., Duan, C., et al., *Dalton Trans.*, 2002, vol. 14, p. 591.
- Rowland, J.M., Thornton, M.L., Olmstead, M.M., and Mascharak, P.K., *Inorg. Chem.*, 2001, vol. 40, p. 1069.
- Qi, J.Y., Ma, H.X., Li, X.J., et al., *Chem. Commun.*, 2003, vol. 11, p. 1294.
- Qi, J.Y., Qiu, L.Q., Lam, K.H., et al., *Chem. Commun.*, 2003, vol. 9, p. 1058.
- Muñiz, K. and Iglesias, A., *Angew. Chem. Int. Ed.*, 2007, vol. 46, p. 6350.
- Fortney, C.F. and Shepherd, R.E., *Inorg. Chem. Commun.*, 2004, vol. 7, p. 1065.
- Wong, C.M., Peterson, M.B., Pernik, I., et al., *Inorg. Chem.*, 2017, vol. 56, p. 14682.
- Busetto, L., Cassani, M.C., Femoni, C., et al., *Organometallics*, 2011, vol. 30, p. 5258.
- Vuong, K.Q., Timerbulatova, M.G., Peterson, M.B., et al., *Dalton Trans.*, 2013, vol. 42, p. 14298.
- Donnelly, K.F., Segarra, C., Shao, L.X., et al., *Organometallics*, 2015, vol. 34, p. 4076.
- Navarro, M., Li, M., Muller-Bunz, H., et al., *Chem. Eur. J.*, 2016, vol. 22, p. 6740.
- Burgess, M.G., Zafar, M.N., Horner, S.T., et al., *Inorg. Chim. Acta*, 2016, vol. 450, p. 124.
- Dragnea, B., Chen, C., Kwak, E.-S., et al., *J. Am. Chem. Soc.*, 2003, vol. 125, p. 6374.
- Braha, O., Walker, B., Cheley, S., et al., *Chem. Biol.*, 1997, vol. 4, p. 497.
- Xiao, Y., Patolsky, F., Katz, E., Hainfeld, J.F., and Willner, I., *Science*, 2003, vol. 299, p. 1877.
- Benson, D.E., Wisz, M.S., and Hellinga, H.W., *Curr. Opin. Biochem.*, 1998, vol. 9, p. 370.
- Lu, Y., Berry, S.M., and Pfister, T.D., *Chem. Rev.*, 2001, vol. 101, p. 3047.
- Straface, A.L., Myers, J.H., Kirchick, H.J., and Blick, K.E., *Am. J. Clin. Pathol.*, 2008, vol. 129, p. 788.
- McCord, J., Nowak, R.M., McCullough, P.A., et al., *Circulation*, 2001, vol. 104, p. 1483.
- Sallach, S.M., Nowak, R., Hudson, M.P., et al., *Am. J. Cardiol.*, 2004, vol. 94, p. 864.
- Apple, F.S., Christenson, R.H., Valdes, R., et al., *Clin. Chem.*, 1999, vol. 45, p. 199.
- Zhang, B., Tamez-Vela, J.M., Solis, S., et al., *Med. Eng.*, 2013, vol. 2013, p. 1.
- Debreczeni, J.E., Bullock, A.N., Atilla, G.E., et al., *Angew. Chem. Int. Ed.*, 2006, vol. 45, p. 1580.
- Lu, Y., *Angew. Chem. Int. Ed.*, 2006, vol. 45, p. 5588.
- Ohashi, M., Koshiyama, T., Ueno, T., et al., *Angew. Chem. Int. Ed.*, 2003, vol. 42, p. 1005.
- Ueno, T., Ohashi, M., Kono, M., et al., *Inorg. Chem.*, 2004, vol. 43, p. 2852.
- Ueno, T., Koshiyama, T., Ohashi, M., et al., *J. Am. Chem. Soc.*, 2005, vol. 127, p. 6556.
- Li, C. and Xiao, J., *J. Am. Chem. Soc.*, 2008, vol. 130, p. 13208.

33. Dürrenberger, M., Heinisch, T., Wilson, Y.M., et al., *Angew. Chem. Int. Ed.*, 2011, vol. 50, p. 3026.
34. Creus, M., Pordea, A., Rossel, T., et al., *Angew. Chem. Int. Ed.*, 2008, vol. 47, p. 1400.
35. Xu, L., Zhu, Q., Huang, G., et al., *J. Org. Chem.*, 2012, vol. 77, p. 3017.
36. Beyramabadi, A. and Morsali, A., *Int. J. Phys. Sci.*, 2011, vol. 6, p. 1780.
37. Monajjemi, M., Sayadian, M., Zare, K., et al., *Int. J. Phys. Sci.*, 2011, vol. 6, p. 4063.
38. Zafar, M.N., Masood, S., Nazar, M.F., et al., *J. Chin. Chem. Soc.*, 2017, vol. 64, p. 1.
39. Epszajn, J. and Jozwiak, A., *Eur. J. Org. Chem.*, 2004, vol. 2004, p. 3254.
40. Velde, G.T., Bickelhaupt, F.M., Gisbergen, S.J.A., et al., *J. Comput. Chem.*, 2001, vol. 22, p. 931.
41. Baerends, E.J., *Amsterdam Density Functional (ADF 2013), Software for Chemistry and Materials (SCM), Theoretical Chemistry*, Amsterdam: Vrije Univ. <http://www.scm.com>.
42. Becke, A.D., *Phys. Rev., A.*, 1998, vol. 38, p. 3098.
43. Lee, C., Yang, W., and Parr, R.G., *Phys. Rev., B: Condens. Matter Mater. Phys.*, 1988, vol. 37, p. 785.
44. Protein Data Bank. <https://www.rcsb.org/pdb/home/home.do>. Accessed December 27, 2017.
45. Doster, M.E. and Johnson, S.A., *Angew. Chem. Int. Ed.*, 2009, vol. 121, p. 2219.
46. Herrmann, W.A., Schütz, J., Frey, G.D., and Herdtweck, E., *Organometallics*, 2006, vol. 25, p. 2437.
47. Wolf, S. and Plenio, H., *J. Orgmet. Chem.*, 2009, vol. 694, p. 1487.
48. Honorio, K.M. and Da Silva, A.B.F., *Int. J. Quant. Chem.*, 2003, vol. 95, p. 126.
49. Li, Y., Yang, M.M., Liu, Y.Y., et al., *J. Mol. Struct.*, 2011, vol. 987, p. 206.
50. Li, Y., Zhang, H., Liu, Y.Y., et al., *J. Mol. Struct.*, 2011, vol. 997, p. 110.
51. Kryger, G., Silman, I., and Sussman, J., *J. Physiol.*, 1998, vol. 92, p. 191.